Master curves and radial distribution functions for shear dilatancy of liquid n -hexadecane via nonequilibrium molecular dynamics simulations

Huan-Chang Tseng, Jiann-Shing Wu, and Rong-Yeu Chang

Citation: The Journal of Chemical Physics **130**, 164515 (2009); doi: 10.1063/1.3123171
View online: http://dx.doi.org/10.1063/1.3123171
View Table of Contents: http://scitation.aip.org/content/aip/journal/jcp/130/16?ver=pdfcov
Published by the AIP Publishing

Master curves and radial distribution functions for shear dilatancy of liquid *n*-hexadecane via nonequilibrium molecular dynamics simulations

Huan-Chang Tseng,[1,a)] Jiann-Shing Wu,[1] and Rong-Yeu Chang[2]
[1]*Department of Applied Chemistry, National Chiao Tung University, Hsinchu, Taiwan 30010, Republic of China*
[2]*Department of Chemical Engineering, National Tsing Hua University, Hsinchu, Taiwan 30043, Republic of China*

(Received 13 November 2008; accepted 29 March 2009; published online 29 April 2009)

Shear dilatancy, a significant nonlinear behavior of nonequilibrium thermodynamics states, has been observed in nonequilibrium molecular dynamics (NEMD) simulations for liquid *n*-hexadecane fluid under extreme shear conditions. The existence of shear dilatancy is relevant to the relationship between the imposed shear rate $\dot{\gamma}$ and the critical shear rate $\dot{\gamma}_c$. Consequently, as $\dot{\gamma} < \dot{\gamma}_c$, the intermolecular equilibrium distance of the fluid remains unchanged, while the nonequilibrium state of the fluid approaches equilibrium. In contrast to $\dot{\gamma} > \dot{\gamma}_c$, the intermolecular distance is lengthened substantially by strong shear deformation breaking the equilibrium thermodynamic state so that shear dilatancy takes place. Notably, a characteristic shear rate $\dot{\gamma}_m$, which depends on the root mean square molecular velocity and the average free molecular distance, is found in nonequilibrium thermodynamics state curves. Studies of the variations in the intermolecular radial distribution function (RDF) with respect to the shear rate provide a direct measure of the variation in the degree of intermolecular separation. Additionally, the variations of the RDF curve in the microscopic regime are consistent with those of the nonequilibrium thermodynamic state in the macroscopic world. By inspecting the overall shape of the RDF curve, it can be readily corroborated that the fluid of interest exists in the *liquid* state. More importantly, both primary characteristic values, the *equilibrium* thermodynamic state variable and a particular shear rate of $\dot{\gamma}_p$, are determined cautiously, with $\dot{\gamma}_p$ depending on the $\dot{\gamma}_m$ value and the *square root* of pressure. Thereby, the nonequilibrium thermodynamic state curves can be normalized as temperature-, pressure-, and density-invariant master curves, formulated by applying the Cross constitutive equation. Clearly, $\dot{\gamma}_c$ occurs at which a reduced shear rate $\dot{\gamma}/\dot{\gamma}_p$ approaches 0.1. Furthermore, the trends in the rates of shear dilatancy in both the constant-pressure and constant-volume NEMD systems under isothermal conditions conform to the *cyclic rule* of pressure, as a function of density and shear rate.
 [DOI: 10.1063/1.3123171]

I. INTRODUCTION

Nonequilibrium molecular dynamics (NEMD) simulations play an important role in helping us understand the relationship between macroscopic transport phenomena and microscopic molecular interactions. Such simulations can integrate thermodynamic states and rheological properties advantageously to explore nonlinear behavior. In NEMD simulations, most simple fluids exhibit a wide variety of non-Newtonian manifestations for rheological investigations, such as *shear thinning phenomena*, *normal stress effects*, and *viscoelastic behaviors*. To date, only a few NEMD discussions regarding nonequilibrium thermodynamics states have appeared in literature.

Shear dilatancy, which is a type of nonlinear behavior in nonequilibrium thermodynamics, is usually observed *under extreme shear* in the field of NEMD research. In general, for rigid particles[1–4] with Lennard–Jones (LJ) and Weeks–Chandler–Andersen (WCA) potential models and for alkane molecules[5–16] and short polymer chains[17–19] with realistic molecular potential models, the shear dilatancy behavior is characterized by a pressure increase in a constant-volume (isochoric-isothermal) NEMD system and by a density decrease in a constant-pressure (isobaric-isothermal) NEMD system when the shear rate is increased. This tendency is generally known as *positive shear dilatancy*;[6,11] negative shear dilatancy (or shear compression) is characterized by the inverse of these trends.[19] For longer molecular chains (length of chain $> \sim 20$ beads), Kröger *et al.*[18] and Xu *et al.*[19] detected *shear compression*, presumably because they created coarse-grained molecular chains by using a finite extensible nonlinear elastic potential to make the chains more flexible. Their studies[18,19] revealed that the overall variations in pressure, with respect to shear rate, depend strongly on the length of the molecular chains; i.e., positive shear dilatancy occurs for shorter chains and negative dilatancy for longer chains.

Reynolds coined the term "dilatancy" in 1885.[8,20] At the time, the dilatancy phenomenon described how the volume of a compacted granular material expanded when it was sheared. Notably, Reiner and Blair[21] suggested the rheologi-

[a)]Author to whom correspondence should be addressed. Electronic mail: ivortseng@moldex3d.com.

cal terminology of related experiments and theories. Because the terms dilatancy and "thickening" were often used interchangeably among practitioners,[8,22] they provided the following technical explanation: Dilatancy is the expanded volume under isobaric-isothermal conditions, but not the increase in viscosity observed for thickening.

Thompson and Grest[23] mimicked granular materials in MD simulations using rigid particles under shear, where a constant loading normal stress and a constant driving velocity were applied in the gradient and flow directions, respectively. Their findings indicated that as the driving velocity was enhanced, an increase in the height of the gradient occurred explicitly. In other words, the expanded volume was significant because of the constant area of the plate, viz., the occurrence of shear dilatancy. Dilatancy phenomenon has been discovered, not only in shear flows of NEMD simulations but also in *elongation* flows, such as the so-called *elongation dilatancy* that emerged in the NEMD simulations of linear-chain polyethylene (PE) liquids by Baig *et al.*,[24] Daivis *et al.*,[25] and Kim *et al.*[26]

During the theoretical development of systems to explain nonlinear fluid behavior, the mode-coupling theory of Kawasaki and Gunton[1,27] confirmed the 3/2 power behavior for shear dilatancy of simple fluids, namely, $P \propto \dot{\gamma}^{3/2}$. Such behavior was demonstrated in the earlier NEMD studies.[1,2] Ge *et al.*[4] recently proposed, however, that the 3/2 power behavior occurs only at the triple point, with a 2.0 power behavior ($P \propto \dot{\gamma}^{2.0}$) existing at common state points; they also proved the existence of both types of behavior through NEMD simulations of LJ and WCA particles. Moreover, Daivis *et al.*[25] studied both the shear dilatancy and elongational dilatancy of polymer melts, using retarded motion expansion (RME) to derive the quadratic term in the strain rates dependence of pressure, where RME (Ref. 28) is a systematic description of rheologically simple viscoelastic fluids having low Deborah numbers. Coincidentally Morriss *et al.*[14] also found the 2.0 power behavior for liquid *n*-decane ($C_{10}H_{22}$) and *n*-eicosane ($C_{20}H_{42}$).

The majority of reports describing constant-volume NEMD simulations have emphasized only the *presence* of shear dilatancy. Some researchers[18,19,26,29–31] have, however, conducted simulations to further analyze the effects of molecular structures on the rate of shear dilatancy. In particular, at a constant molecular weight of 100 *methylene* (CH_2) beads, Jabbarzadeh *et al.*[29] showed that the rate of shear dilatancy was not related to the molecular structure of H, star, comb, and branched architectures, whereas an investigation of different molecular weights performed by Bosko *et al.*[30] revealed that the rate of shear dilatancy increased upon increasing the degree of branching. Moreover, in constant-volume NEMD systems, the variation of pressure is relevant to both the intermolecular LJ and torsion potentials; this relationship is completely discussed in several articles[6,17,26] regarding changes in intermolecular and intramolecular potentials with respect to the shear rate. Notably, using a pair-correlation function (or radial distribution function), Koo and Hess[32] found that the molecular origin of shear dilatancy was ellipsoidal distortion of the pair-correlation function at lower shear rates and twisted distortion at higher shear rates; such results are consistent with related experimental observations.[33,34]

Most published NEMD studies concerning shear dilatancy have been limited to constant-volume NEMD systems; such studies may not be convenient in related applications since experimental data are usually measured under *isobaric* conditions.[5,9,31] Regrettably, only a few attempts have been made to probe constant-pressure NEMD simulations[8,10,15,19,31] because of issues relating to numerical instability: The instantaneous pressure drifts suddenly to generate large instantaneous volume fluctuations.[35] To resolve this issue, Wang and Fichthorn[35] proposed a modified pressure method to obtain an effectively stable numerical solution of the volume.

Judging from literature cited above, NEMD discussions with respect to nonequilibrium thermodynamic states have almost invariably stressed (i) the observation of shear dilatancy behavior or (ii) how this behavior as related to the intermolecular LJ potential; at best, we have only a limited understanding of how shear dilatancy is affected by changes in molecular structure. Recently, in NEMD studies of liquid *n*-hexadecane ($C_{16}H_{34}$), we found[16] that the rate of shear dilatancy decreased *strongly* upon increasing the pressure and density, whereas it increased only *weakly* upon increasing the temperature. In addition, variations in the degrees of shear dilatancy are qualitatively contrary to those of shear thinning.[16,36] The reasons for shear dilatancy occurring in NEMD simulations have not, however, been addressed previously from a molecular point of view.

Our objective for this present study was to determine the probable cause of shear dilatancy in NEMD simulations, as related to the imposed shear rate and the root mean square molecular velocity, based on our previous study.[16] Thus, we cautiously normalized the nonequilibrium thermodynamic state curves into the form of master curves—temperature, pressure, and density invariant—using two characteristic values: A thermodynamic state variable and a particular shear rate. Interestingly, we could extend the thermodynamic space in terms of four variables, namely temperature (T), pressure (P), density (ρ), and shear rate ($\dot{\gamma}$). Considering that the rates of shear dilatancy in both constant-volume and constant-pressure NEMD systems under isothermal conditions are $(\partial P/\partial \dot{\gamma})_{T,\rho}$ and $(\partial \rho/\partial \dot{\gamma})_{T,P}$, respectively, we further examined whether or not their tendencies conformed to the *cyclic rule*[2,37] of the pressure as a function of density and shear rate.

More importantly, we used the radial distribution function (RDF) to understand how the change in the intermolecular distance was related to that in the nonequilibrium thermodynamic state. Also, we investigated how the RDF curves were affected by the temperature, pressure, density, and shear rate. Furthermore, we could use the overall shape of the RDF curve to validate that our research fluid existed in the liquid state.

In Sec. II, we briefly describe the necessary theoretical background; in Sec. III, we present our results related to the abovementioned studies; in Sec. IV, we summarize the main conclusions and suggest future studies.

II. SIMULATION DETAILS

In a previous study,[16] we investigated the shear thinning and shear dilatancy behaviors of liquid *n*-hexadecane through NEMD simulations. For completeness, here the potential models and simulation algorithms used in this present study are briefly summarized. Our molecular modeling was based on the set of realistic potential models described by Chynoweth and Michopoulos (CM),[38,39] who fit the optimal parameters of the van der Waals (vdW) potential by adopting experimental data of heat enthalpy of vaporization. As a whole, the CM model was better at quantitatively predicting the rheological properties of shear flows[16] than was the transferable potential for phase equilibria (TraPPE) model,[40] which is an adaptation applied in predictions of equilibrium thermodynamic properties to calculate the vapor-liquid coexistence curves[41] and surface tensions[42] of *n*-alkane phase diagrams. On the other hand, when predicting thermodynamic properties, the TraPPE model is superior[16] to the CM model.

The CM model describes how the molecular chain is modeled with the use of spherical interaction sites, regarded as *methylene* (CH_2) groups. Interaction sites connected together can form molecular chains through dominant vdW and covalent bonding interactions, providing the bond stretching, bond bending, and torsion motions of molecules. The functions and parameters of those potentials for the CM model are the same as the ones we apply to model *n*-hexadecane molecule.[16] This model has been adopted previously in the steady state shear flow,[16,36,43–45] oscillatory shear flow,[46] and contraction flow[47] portions of molecular dynamics simulations.

The NEMD algorithm[48–50] was originally developed by combining SLLOD equations of motion with the Lees–Edwards sliding brick periodic boundary condition.[51] In this present study, we performed our NEMD simulations under isothermal conditions involving both constant-volume NEMD (*NVT*-NEMD) and constant-pressure[8,10] NEMD (*NPT*-NEMD) systems. As for the whole simulation framework, we chose the *atomic version*, including the SLLOD equations of motion, temperature, and stress tensor. In addition, the isothermal NEMD systems were achieved by using the atomic Gaussian thermostat method.[48–50] For a suitable range of shear rates ($\dot{\gamma} < 1.1 \times 10^{12}$ s^{-1}; 2.5 in reduced units), the atomic thermostat caused no strange effects in the predictions of the thermodynamic states and rheological properties.[29,52] Recently, Daivis reported that the nonlinear behavior observed in NEMD simulations was influenced by the specific thermostat methods used for shearing linear viscoelastic fluids.[53]

Furthermore, the SLLOD equations can be implemented using MacGowan and Heyes' Leapfrog–Verlet scheme,[54] which offers a fast converging *iterative* algorithm for Gaussian thermostat multipliers.[5] The magnitude of the time step (from 1.0 to 0.1 fs) depends on a shear rate. After the simulation system approaches a steady state (typically several million time steps), the atomic trajectories are collected and calculated using time averages. Detailed information regarding the molecular potentials, SLLOD algorithms, and other related methods are available elsewhere.[16]

Significantly, the radial distribution function, one of the focuses of our present study, can be applied indirectly to explore the intermolecular behavior of shear dilatancy. The radial distribution function, generally abbreviated $g(r)$ with the understanding that it describes the probability of finding two molecules at a separation distance r, is defined[49,55–58] as the ratio of the local number density at a distance r from the central molecule to the bulk number density

$$g(r) = \frac{\langle \Sigma_{i=1}^{N} \Sigma_{j>i}^{N} \delta(|\mathbf{r} - \mathbf{r}_{ij}|) \rangle}{4\pi r^2 N \rho}, \tag{1}$$

where $\mathbf{r}$ is the orientation of the separation vector with its distance r, $\mathbf{r}_{ij}$ is the distance vector between the centers of mass of molecules i and j, N is the total number of molecules, ρ is the density, and δ is the delta symbol;[55] the angled brackets denote the time average.

Note that the radial distribution function is also as a function of density ρ and temperature T, namely, $g(r,\rho,T)$. For a pure fluid, $g(r,\rho,T)$ must satisfy the following asymptotic relations: (1) In the *ideal gas* state, i.e., as ρ approaches *zero*, $\lim_{\rho \to 0} g(r,\rho,T) = 1$; (2) at a *large* intermolecular distance, $\lim_{r \to \infty} g(r,\rho,T) = 1$.[57] In general, the characteristics of $g(r)$ curves can be useful to distinguish between the three phase states (gas, liquid, and solid) of a pure fluid.[59] Experimentally, $g(r)$ can be obtained from x-ray or neutron-scattering measurements of gases and liquids.[56] In this present study, we examined the effects of temperature, pressure, density, and shear rate on the resulting $g(r)$ curves.

III. RESULTS AND DISCUSSION

Following our earlier study,[16] liquid *n*-hexadecane was steadily sheared over a wide range of shear rates (from $1 \times 10^{9.0}$ to $1 \times 10^{12.0}$ s^{-1}). The flow (x-axis) and gradient (y-axis) directional sizes (L_x and L_y, respectively) of the simple shear flow system were 3.0 and 4.5 nm, respectively. Our research fluid consisted of 144 *n*-hexadecane molecules. A shear rate $\dot{\gamma}$ was applied to the fluid to characterize the shear flow field; $\dot{\gamma}$ is related to the streaming velocity v_x in the x direction, namely, $\dot{\gamma} = \partial v_x / \partial y$. The *periodic boundary condition* was adopted in *all* directions while "the Lees–Edwards boundary condition" was used in the xy plane.[49,50] To determine the possible reasons for shear dilatancy occurring in NEMD simulations, the first goal of our present study was to propose an explanation from the molecular point of view. The second—and major—goal was to carefully normalize the nonequilibrium thermodynamic state curves under different temperatures, pressures, and densities as temperature-, pressure-, and density-invariant master curves, respectively. These master curves were formally described using the Cross constitutive equation.[28] Incidentally, we found that the rate of shear dilatancy in both constant-pressure and constant-volume NEMD systems conformed to the *cyclic rule*[2,37] of the pressure, i.e., as a function of the density and shear rate. Our third goal was to verify whether or not the changes in RDF (Refs. 55–57) with respect to the shear rate were related to the shear dilatancy. In addition, we examined how the temperature, pressure, and density influ-

TABLE I. Temperature dependence of various parameters for normalized $\rho-\dot{\gamma}$ curves at 250 MPa in *NPT*-NEMD simulations.

T (K)	300	350	400	450	500
ρ_e (g/cm^3)[a]	0.836	0.818	0.801	0.785	0.770
$\dot{\gamma}_c$ (s^{-1})	$4.0\times10^{10.0}$	$4.4\times10^{10.0}$	$4.7\times10^{10.0}$	$5.0\times10^{10.0}$	$5.2\times10^{10.0}$
$\bar{v}_{\mathrm{rms}}$ (m/s)	181.8	196.4	209.9	222.6	234.7
l_m (Å)	7.663	7.719	7.773	7.825	7.876
$\dot{\gamma}_m$ (s^{-1})	$2.37\times10^{11.0}$	$2.54\times10^{11.0}$	$2.70\times10^{11.0}$	$2.85\times10^{11.0}$	$2.98\times10^{11.0}$

[a]Taken from Ref. 16.

enced the radial distribution function. Simultaneously, we confirmed that our fluid of interest, *n*-hexadecane, existed in the liquid state by observing a curve characteristic of a RDF.

A. Molecular explanation of shear dilatancy

Before the moment at which shear dilatancy occurs can be determined, two issues must be resolved: (i) At low shear rates, why does the variation of the nonequilibrium thermodynamic state, with respect to the shear rate, approach a convergent equilibrium state? In contrast, at high shear rates, why does shear dilatancy occur?; and (ii) One *deviation point* defines the onset of the nonequilibrium thermodynamic state curve's deviation from the convergence state; thus, what is the possible physical meaning of this deviation point, and how is it affected by temperature, pressure, and density? A detailed response to these questions follows.

Shear deformation was exerted upon the *n*-hexadecane molecules by the fluid itself. When the imposed shear rate ($\dot{\gamma}$) was obviously less than a critical shear rate ($\dot{\gamma}_c$), the intermolecular separation did not change explicitly. In this situation, the corresponding thermodynamic state of the fluid was not affected by shear deformation.

In contrast, when $\dot{\gamma}>\dot{\gamma}_c$ (i.e., the fluid was strongly sheared), it appeared that the separation distance was altered and, as a result, that shear dilatancy occurred. In constant-pressure NEMD simulations, the density decreased upon increasing the shear rate;[16] this behavior implied that the intermolecular separation would increase upon decreasing the density. Therefore, for shear dilatancy, the intermolecular separation would increase as the shear rate increased. In Sec. III C, we describe how we used a RDF to confirm this behavior. Consequently, the moment at which shear dilatancy occurred in NEMD simulations was connected to the relationship between $\dot{\gamma}$ and $\dot{\gamma}_c$. Thus, we have clarified the cause of the first issue raised above.

It is worth nothing that, in a previous study,[16] we found that a *transient point* existed in the density–shear rate ($\rho-\dot{\gamma}$) curve of the constant-pressure NEMD simulations at $\dot{\gamma}\approx1\times10^{11.0}$ s^{-1}, and followed the slope of shear dilatancy from the convergent density plateau region. By imagining a dashed horizontal line marked on the convergent density, a *deviation point* can be identified roughly between $1\times10^{10.5}$ and $1\times10^{11.0}$ s^{-1}. This deviation point corresponds to a particular shear rate, i.e., the onset of shear dilatancy, also known as critical shear rate, $\dot{\gamma}_c$.

We observed that the $\dot{\gamma}_c$ value increased gradually upon increasing the temperature; in contrast, the $\dot{\gamma}_c$ value did not depend on pressure.[16] Similar to the results obtained for the constant-pressure NEMD simulations, the pressure–shear rate ($P-\dot{\gamma}$) curves of the constant-volume NEMD simulations revealed that the values of $\dot{\gamma}_c$ were not related to density.

According to elementary statistical mechanics, when certain molecules exist at a constant temperature T, the root mean square molecular velocity[37] $\bar{v}_{\mathrm{rms}}$ is derived by

$$\bar{v}_{\mathrm{rms}}=\sqrt{\frac{3k_BT}{M}}, \tag{2}$$

where k_B is Boltzmann's constant (1.381×10^{-23} J/K) and M is the molecular weight. The molecular weight of *n*-hexadecane is 226.44 g/mol. Table I lists the values of $\bar{v}_{\mathrm{rms}}$ obtained at various temperatures within the temperature range of 300–500 K.

Because $\dot{\gamma}_c$ and $\bar{v}_{\mathrm{rms}}$ were relative to temperature, we presumed, albeit cautiously, that $\dot{\gamma}_c$ might depend on $\bar{v}_{\mathrm{rms}}$. Table I lists the values of $\dot{\gamma}_c$ for *n*-hexadecane at various temperatures within the range of 300–500 K. Thus, the second issue, as described above, has also been resolved.

In summary, we suggest the following simple rule of shear dilatancy: If $\dot{\gamma}>\dot{\gamma}_c$, the substantial motion of the molecules will be affected so that the disrupted fluid's equilibrium thermodynamic state also results in shear dilatancy. The existence of shear dilatancy thus depends on the values of $\dot{\gamma}$ and $\dot{\gamma}_c$, where $\dot{\gamma}_c$ has a connection with $\bar{v}_{\mathrm{rms}}$ depending on temperature. As a consequence, $\dot{\gamma}_c$ increases upon increasing the temperature, whereas pressure and density have no evident effect. Significantly, in Sec. III B we will precisely determine the magnitude of $\dot{\gamma}_c$ in reduced units when deriving a characteristic shear rate.

From rheological considerations,[28] we would initially attempt to find a characteristic shear rate $\dot{\gamma}_m$ depending on $\bar{v}_{\mathrm{rms}}$, as

$$\dot{\gamma}_m=\frac{\bar{v}_{\mathrm{rms}}}{l_m}, \tag{3}$$

where l_m is a average free distance of molecules, namely, $l_m=(V/N)^{1/3}=(M/\rho_e)^{1/3}$; ρ_e is the equilibrium density of *n*-hexadecane fluid and its volume V contains N *n*-hexadecane molecules.

Notably, the definition of $\dot{\gamma}_m$ in Eq. (3) implies that the critical shear rate for the onset of shear dilatancy depends on the average free molecular distance. Generally speaking, the critical shear rate of viscosity–shear rate ($\eta-\dot{\gamma}$) curves is interpreted in terms of viscoelastic relaxation time τ_R.[60] Furthermore, the relaxation time for shear dilatancy, τ_{SD}, may not be the same as τ_R and, so, not expected to depend on the

system size. Thereby, our present study indicates that for a fixed system size, τ_{SD} should depend obviously on temperature.

B. Master curves for shear dilatancy

In macroscopic rheological experiments,[28] the viscosity–shear rate $(\eta-\dot{\gamma})$ flow curves obtained at different temperatures can usually be normalized to provide a master curve through a *shift factor* of time–temperature superposition.[61] Some NEMD studies[13,39,62,63] have also revealed that flow curves at *different state points* can be reduced to a master curve. In addition, we recently reported three types of $\eta-\dot{\gamma}$ master curves—namely, temperature, pressure, and density invariant.[36] Because the overall shape of the nonequilibrium thermodynamic state curves were similar to those of the $\eta-\dot{\gamma}$ flow curves, in this study we also sought to obtain master curves from the nonequilibrium thermodynamic state curves.

Prior to obtaining the master curves for the nonequilibrium thermodynamic state curves,[16] it was important for us to determine two characteristic values: The thermodynamic state and the shear rate variables. The density-characteristic value ρ_C in constant-pressure NEMD systems is given by the equilibrium density ρ_e, whereas the pressure-characteristic value P_C in constant-volume NEMD systems is given by the equilibrium pressure P_e; namely, $\rho_C=\rho_e$ and $P_C=P_e$, respectively. Additionally, $\dot{\gamma}_m$ was selected *initially* as the shear rate characteristic value, as referred to Eq. (3).

Next, using those characteristic values, we normalized the nonequilibrium thermodynamic state curves at various temperatures, pressures, and densities to achieve the temperature-, pressure-, and density-invariant master curves, respectively. Significantly, under isothermal conditions, we could simply inspect whether or not the tendencies of the rate of shear dilatancy in both constant-pressure and constant-volume NEMD systems conformed to the *cyclic rule*[2,37] of pressure, which is a function of density and shear rate.

1. Temperature-invariant master curve

The melting point[59] and boiling point[38] of *n*-hexadecane are 289–291 and 558 K, respectively. Therefore, it was assumed that the fluid in this present study existed in the liquid state at a temperature between 300 and 500 K.

After having referred to a previous study,[16] we performed $\rho-\dot{\gamma}$ curves of nonequilibrium thermodynamic state in *NPT*-NEMD simulations for *n*-hexadecane fluid at 250 MPa and five different temperatures (300, 350, 400, 450, and 500 K). Thereby, Table I lists the characteristic values of ρ_e and $\dot{\gamma}_m$ with respect to the temperature. We further reduced the $\rho-\dot{\gamma}$ curves at different temperatures via ρ_e and $\dot{\gamma}_m$, as shown in Fig. 1. Surprisingly, the plots of ρ/ρ_e versus $\dot{\gamma}/\dot{\gamma}_m$ at various temperatures were all superimposable. We successfully obtained the temperature-invariant master curve. In addition, the master curve could then be formally described formally using the Cross constitutive equation below, as a function of density and shear rate,[28]

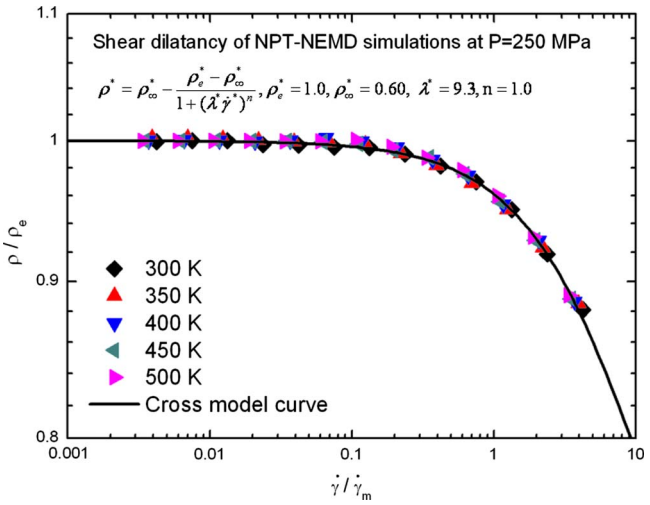

FIG. 1. (Color online) Temperature-invariant master curve for dimensionless density ρ/ρ_e as a function of dimensionless shear rate $\dot{\gamma}/\dot{\gamma}_m$, as obtained from *NPT*-NEMD simulations for *n*-hexadecane at 250 MPa and temperatures between 300 and 500 K. Solid line: Cross model curve fitted to the data.

$$\rho^* = \rho^*_\infty + \frac{\rho^*_e - \rho^*_\infty}{1+(\lambda^*\dot{\gamma}^*)^n}, \tag{4}$$

where $\rho^*=\rho/\rho_e$, $\rho^*_e=\rho_e/\rho_e$, $\rho^*_\infty=\rho_\infty/\rho_e$, $\lambda^*=\lambda\dot{\gamma}_m$, and $\dot{\gamma}^*=\dot{\gamma}/\dot{\gamma}_m$. This equation has four parameters: ρ^*_e, ρ^*_∞, λ^*, and n. After fitting the data, the parameters of the Cross model in Eq. (4) for the temperature-invariant master curve were $\rho^*_e=1.0$, $\rho^*_\infty=0.60$, $\lambda^*=9.3$, and $n=1.0$. The Cross model curve, which is the solid line in Fig. 1, accurately passes through the centers of all the reduced points and is a good representation of the temperature-invariant $\rho-\dot{\gamma}$ master curve. Note that $\dot{\gamma}_c$ obviously occurs at $\dot{\gamma}/\dot{\gamma}_p \approx 0.1$; as $\dot{\gamma}/\dot{\gamma}_p \leq 0.1$, the nonequilibrium thermodynamic state approaches equilibrium.

2. Pressure-invariant master curve

In our previous study,[16] we obtained $\rho-\dot{\gamma}$ curves from *NPT*-NEMD simulations of liquid *n*-hexadecane at 400 K

TABLE II. Pressure dependence of various parameters for normalized $\rho-\dot{\gamma}$ curves at 400 K in *NPT*-NEMD simulations.

P (MPa)	50	100	250	500	750	1000
ρ_e (g/cm^3)[a]	0.699	0.737	0.801	0.866	0.911	0.950
l_m (Å)	8.134	7.992	7.773	7.573	7.446	7.343
$\dot{\gamma}_m$ (s^{-1})	$2.58\times10^{11.0}$	$2.63\times10^{11.0}$	$2.70\times10^{11.0}$	$2.77\times10^{11.0}$	$2.82\times10^{11.0}$	$2.86\times10^{11.0}$
a_p	0.447	0.632	1.000	1.414	1.732	2.000
$\dot{\gamma}_p$ (s^{-1})	$5.77\times10^{11.0}$	$4.15\times10^{11.0}$	$2.70\times10^{11.0}$	$1.96\times10^{11.0}$	$1.63\times10^{11.0}$	$1.43\times10^{11.0}$

[a]Taken from Ref. 16.

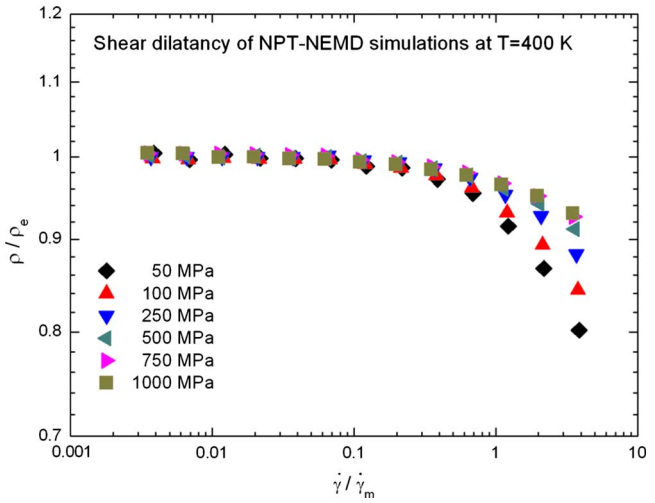

FIG. 2. (Color online) Normalized plots of dimensionless density ρ/ρ_e vs dimensionless shear rate $\dot{\gamma}/\dot{\gamma}_m$, as obtained from *NPT*-NEMD simulations for *n*-hexadecane at 400 K and pressures between 50 and 1000 MPa.

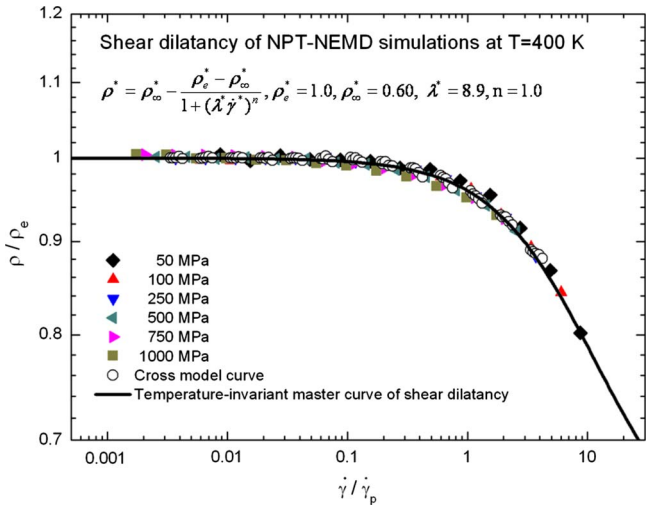

FIG. 3. (Color online) Pressure-invariant master curve for dimensionless density ρ/ρ_e as a function of dimensionless shear rate $\dot{\gamma}/\dot{\gamma}_p$, as obtained from *NPT*-NEMD simulations for *n*-hexadecane at 400 K and pressures between 50 and 1000 MPa. Data taken at the indicated pressures were shifted to a reference pressure, $P_0=250$ MPa. Solid line: Cross model curve fitted to the data. The open square symbols: The ρ/ρ_e vs $\dot{\gamma}/\dot{\gamma}_m$ data of the temperature-invariant master curve were caught from Fig. 1.

over a wide range of pressure (50–1000 MPa). Table II lists the values of ρ_e and $\dot{\gamma}_m$ with respect to pressure. Thus, the $\rho-\dot{\gamma}$ curves at different pressures can be reduced to dimensionless units by ρ_e and $\dot{\gamma}_m$. Figure 2 displays ρ/ρ_e plotted as a function of $\dot{\gamma}/\dot{\gamma}_m$. Dramatically, for $\dot{\gamma}/\dot{\gamma}_m>0.1$, the reduced curves of ρ/ρ_e versus $\dot{\gamma}/\dot{\gamma}_m$ were *not* superimposable. This result suggested that the slope of the shear dilatancy strongly depended on pressure;[16] nevertheless, the overall reduced curves were all rather similar. We applied a *shift factor* a_P of the *time–temperature superposition*[28,61]—a concept adapted from polymer physics—to the reduced curves in the present study. When the reference pressure P_0 was set to 250 MPa, we could use the shift factors to move the other curves to the curve obtained at the reference pressure. Using this approach, we might have expected to obtain one master curve at a reference pressure of 250 MPa. Indeed, a *new* shear rate characteristic value $\dot{\gamma}_p$ that was dependent on pressure can be defined by adjusting $\dot{\gamma}_m$ as follows:

$$\dot{\gamma}_p = a_p \dot{\gamma}_m. \tag{5}$$

An additional question then presented itself: What was the value of a_P when only the pressure P was a function of the shear rate $\dot{\gamma}$? Notably, from an NEMD study, Ge *et al.*[4] reported that, whereas sheared simple fluids at a triple point exhibited a 3/2 power behavior ($P\propto\dot{\gamma}^{3/2}$), those at common states possessed a 2.0 power behavior ($P\propto\dot{\gamma}^{2.0}$). More Recently, Daivis *et al.*[25] employed "the third-order retarded motion expansion of continuum mechanics" to derive the quadratic term in the strain rates dependence of pressure. In an earlier NEMD study of liquid *n*-decane ($C_{10}H_{22}$) and *n*-eicosane ($C_{20}H_{42}$), Morriss *et al.*[14] also found such 2.0 power behavior. From these precedents, we assumed, with caution, that $\dot{\gamma}\propto\sqrt{P}$ could be employed in the present study. Such proportionality resulted in a_P being defined as

$$a_p = \sqrt{\frac{P}{P_0}}. \tag{6}$$

Accordingly, using Eq. (5), we calculated the values of $\dot{\gamma}_p$ at various pressures under a reference pressure of 250 MPa; Table II lists the values of a_P and $\dot{\gamma}_p$ with respect to pressure. Figure 3 presents ρ/ρ_e plotted with respect to $\dot{\gamma}/\dot{\gamma}_p$. Surprisingly, at an isothermal temperature of 400 K and a reference pressure of 250 MPa, the master curve was obtained via the use of a shift factor. Then, this master curve can also be well described using the Cross model, Eq. (4), with the following parameters: $\rho_e^*=1.0$, $\rho_\infty^*=0.60$, $\lambda^*=8.9$, and $n=1.0$, where the reduced shear rate $\dot{\gamma}^*$ and the reduced relaxation time λ^* have been modified as $\dot{\gamma}^*=\dot{\gamma}/\dot{\gamma}_p$ and $\lambda^*=\lambda\dot{\gamma}_p$. In Fig. 3, the solid curve is the Cross model curve and the open square symbols represent the reduced data of ρ/ρ_e versus $\dot{\gamma}/\dot{\gamma}_m$ captured from the temperature-invariant master curve at 250 MPa, as in Fig. 1. These two plots are almost superimposable. As a result, findings presented in Figs. 1 and 3 at the same temperature (400 K) and pressure (250 MPa) are in good agreement, with the parameters of their Cross model curves being fairly close in value. Similar to Fig. 1, $\dot{\gamma}_c$ in Fig. 3 also occurs at $\dot{\gamma}/\dot{\gamma}_p\approx0.1$.

Here, an explanation is necessary as to why Fig. 2 showing the pressure effect using "the value of $\dot{\gamma}_m$" is *not* similar to Fig. 1 showing the temperature effect. In a previous study,[16] we fitted the $\rho-\dot{\gamma}$ curves between $1\times10^{11.0}$ and $1\times10^{12.0}$ s^{-1} to the power-law model[16,19] $\rho\propto\dot{\gamma}^{-n_\rho}$, where n_ρ is an exponent for shear dilatancy in a constant-pressure NEMD system; this exponent also implicitly relates to the rate of shear dilatancy. As a consequence, we obtained the following values of n_ρ at various temperatures: 0.070 (300 K), 0.076 (350 K), 0.082 (400 K), 0.089 (450 K), and 0.095 (500 K);[16] at various pressures, the values of n_ρ were 0.241 (50 MPa), 0.162 (100 MPa), 0.082 (250 MPa), 0.065 (500 MPa), 0.053 (750 MPa), and 0.046 (1000 MPa).[16] Overall, this tendency suggested that the value of n_ρ *decreased dramatically* upon increasing the pressure; the increase in n_ρ upon increasing the temperature was less obvious. In other words, the shear dilatancy behavior was *strongly* related to

TABLE III. Density dependence of various parameters for normalized $P-\dot{\gamma}$ curves at 400 K in *NVT*-NEMD simulations.

ρ (g/cm^3)	0.70	0.75	0.80	0.85	0.90
P_e (MPa)[a]	66.3	140.6	258.9	440.9	698.6
l_m (Å)	8.130	7.945	7.776	7.620	7.477
$\dot{\gamma}_m$ (s^{-1})	$2.58\times10^{11.0}$	$2.64\times10^{11.0}$	$2.70\times10^{11.0}$	$2.75\times10^{11.0}$	$2.81\times10^{11.0}$
a_p	0.506	0.737	1.000	1.305	1.643
$\dot{\gamma}_p$ (s^{-1})	$1.31\times10^{11.0}$	$1.95\times10^{11.0}$	$2.70\times10^{11.0}$	$3.59\times10^{11.0}$	$4.61\times10^{11.0}$

[a]Taken from Ref. 16.

pressure, but only *weakly* to temperature. Therefore, we expected the results presented in Fig. 2 to differ from those in Fig. 1 for the same value of $\dot{\gamma}_m$ used.

3. Density-invariant master curve

In the liquid/vapor coexistence curve of *n*-hexadecane, the phase diagram at 400 K reveals a liquid state density of greater than 0.65 g/cm^3; in contrast, at less than 0.65 g/cm^3, the fluid comprises coexisting liquid and vapor states.[16] To ensure that our simulated fluid existed well within the region of a single liquid phase, we chose the following five densities for the *n*-hexadecane fluid in our *NVT*-NEMD simulations performed at 400 K: 0.70, 0.75, 0.80, 0.85, and 0.90 g/cm^3. The $P-\dot{\gamma}$ plot is available in our previous publication.[16]

Table III lists the values of P_e and $\dot{\gamma}_m$ with respect to density. Figure 4 presents P/P_e plotted with respect to $\dot{\gamma}/\dot{\gamma}_m$. Similar to Fig. 2, at $\dot{\gamma}/\dot{\gamma}_m > 0.1$, the reduced curves of P/P_e versus $\dot{\gamma}/\dot{\gamma}_m$ were also not obviously superimposable, which suggested that the slope of the plot of the shear dilatancy was strongly affected by density. Because pressure and density have parallel effects on shear dilatancy,[16] the reduced curves obtained at various densities were also readily transformed—through a shift factor—to that at the reference density; this approach was identical to that we described for the pressure effect in Sec. III B 2.

Thus, we chose a reference density ρ_0 and determined its corresponding pressure $P(\rho_0)$. We used a shift factor, $a_p = \sqrt{P_e(\rho)/P_e(\rho_0)}$, to obtain the value of $\dot{\gamma}_p$. For the reference density $\rho_0 = 0.80$ g/cm^3, Table III lists both the values of a_P and $\dot{\gamma}_p$ with respect to density. As expected, Fig. 5 shows that the corresponding master curve of P/P_e versus $\dot{\gamma}/\dot{\gamma}_p$ was obtained at an isothermal temperature of 400 K and a reference density of 0.80 g/cm^3. In addition, we also formulated this master curve using the Cross model below, as a function of pressure and shear rate,

$$P^* = P^*_\infty + \frac{P^*_e - P^*_\infty}{1 + (\lambda^* \dot{\gamma}^*)^n}, \tag{7}$$

where $P^* = P/P_e$, $P^*_e = P_e/P_e$, $P^*_\infty = P_\infty/P_e$, $\lambda^* = \lambda\dot{\gamma}_p$, and $\dot{\gamma}^* = \dot{\gamma}/\dot{\gamma}_p$. This equation has four parameters: P^*_e, P^*_∞, λ^*, and n. The solid curve in Fig. 5 is the Cross model curve of Eq. (7) drawn with the following parameters: $P^*_e = 1.0$, $P^*_\infty = 30.0$, $\lambda^* = 72.7$, and $n = 1.0$. This model curve passed well through the overall center of the data. As expected, in Fig. 5, $\dot{\gamma}_c$ is also found at $\dot{\gamma}/\dot{\gamma}_p \approx 0.1$. The nonequilibrium pressure at $\dot{\gamma}/\dot{\gamma}_p \leq 0.1$ is closer to the equilibrium value.

More importantly, we focused our attention on understanding why the pressure increased upon increasing the shear rate, especially in constant-volume NEMD simulations at high shear rates. From a microscopic viewpoint, atomic pressure[49,55] is a function of the *kinetic* energy E_k and the *virial* energy E_{virial}, which are related to the temperature and

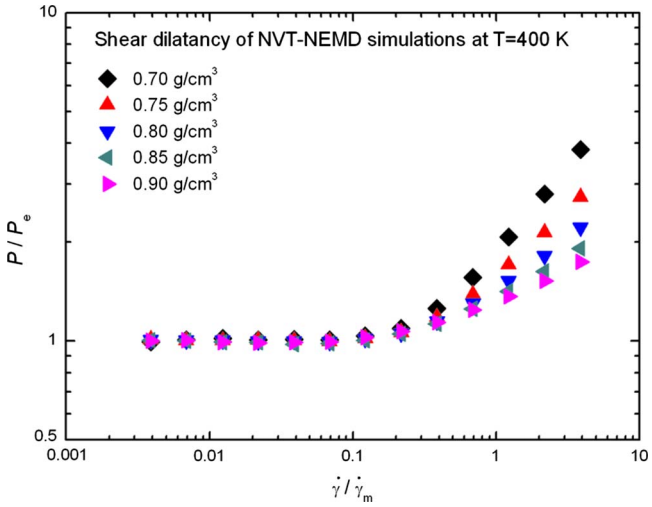

FIG. 4. (Color online) Normalized plots of dimensionless pressure P/P_e vs dimensionless shear rate $\dot{\gamma}/\dot{\gamma}_m$, as obtained from *NVT*-NEMD simulations for *n*-hexadecane at 400 K and densities between 0.70 and 0.90 g/cm^3.

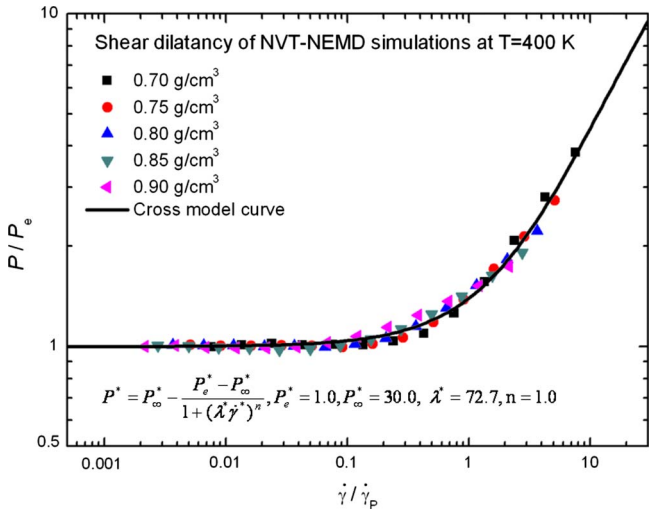

FIG. 5. (Color online) Density-invariant master curve for dimensionless pressure P/P_e as a function of dimensionless shear rate $\dot{\gamma}/\dot{\gamma}_p$, as obtained from *NVT*-NEMD simulations for *n*-hexadecane at 400 K and densities between 0.70 and 0.90 g/cm^3. Data taken at the indicated densities were shifted to a reference density, $\rho_0 = 0.80$ g/cm^3. Solid line: Cross model curve fitted to the data.

potential energy, respectively. Because E_k is held constant at an isothermal temperature of 400 K, E_{virial} plays a dominant role in determining the variation of pressure. In most cases, E_{virial} has a negative value. When molecular chains readily exclude one another, so that the E_{virial} value is enhanced, the pressure rises accordingly. Moore *et al.*[13] suggested that when a strong shear deformation is imposed onto a fluid at an extreme shear rate, the intermolecular collisions are more frequent and stronger, i.e., a Brownian-type collision effect.[13,26] In such a state, we would infer that the increase in the intermolecular distance would make it more difficult for the molecules to interact, causing the pressure to increase upon increasing the value of E_{virial}. In Sec. III C, whether by constant-volume or constant-pressure NEMD simulations, we validated, through variations in the RDF with respect to the shear rate, that shear dilatancy behavior caused an increase in the intermolecular distance.

Moreover, it is interesting to note that extended thermodynamic space is considered to be a function of four variables: Temperature T, pressure P, density ρ, and shear rate $\dot{\gamma}$. Under isothermal conditions, pressure is an *exact function* of density and the shear rate: $P=P(\rho,\dot{\gamma})$; therefore, we obtained the *cyclic rule*[2,37] via the total differential of $P=P(\rho,\dot{\gamma})$

$$\left(\frac{\partial P}{\partial \dot{\gamma}}\right)_{T,\rho} = -\left(\frac{\partial P}{\partial \rho}\right)_{T,\dot{\gamma}}\left(\frac{\partial \rho}{\partial \dot{\gamma}}\right)_{T,P}. \tag{8}$$

The shear dilatancy aspect of the constant-pressure NEMD simulations, as presented in Figs. 1 and 3, clearly indicated that $(\partial\rho/\partial\dot{\gamma})_{T,P}<0$. Additionally, in our previous study,[16] under a constant temperature (400 K) and shear rate $(1\times10^{12.0}\ \text{s}^{-1})$, we observed that $(\partial P/\partial\rho)_{T,\dot{\gamma}}>0$; thus, as in, Eq. (8), $(\partial P/\partial\dot{\gamma})_{T,\rho}>0$. This indirect ratiocination was in good agreement with our observations of the shear dilatancy aspect of the constant-volume NEMD simulations in Fig. 5. As a whole, our results above have firmly supported the validity of shear dilatancy in both constant-volume and constant-pressure NEMD simulations. In particular, it has been suggested that Eq. (8) is true for *a unique thermodynamic temperature* in the shearing steady state system; however, the validity of this assumption is questionable and it has recently been challenged. We refer the reader to previous studies, discussed by Daivis[53,64] and Matin,[64] regarding the thermodynamic relationships of shearing linear viscoelastic fluids.

C. Radial distribution functions for intermolecules

Above, we have described how we obtained master curves from nonequilibrium thermodynamics state curves; in addition, we corroborated our supposition for shear dilatancy, i.e., that the intermolecular separation increased upon increasing the shear rate. In this section, using RDFs,[49,55–58] we show that variations in the intermolecular distance are related to shear dilatancy. The RDF is the primary linkage between macroscopic thermodynamic properties and intermolecular interactions within fluids. Hence, not only could we analyze the variation in the intermolecular distance in terms of the effects of temperature, pressure, density, and shear rate but we could also manifest with certainty that our research fluid existed in a liquid state.

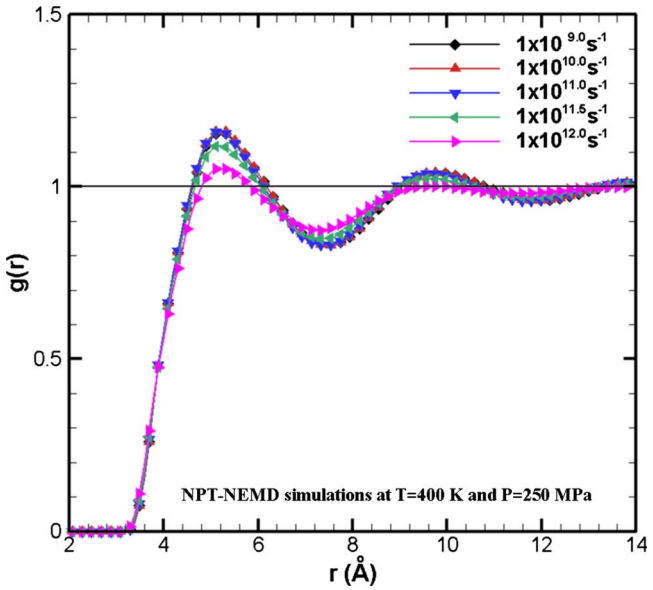

FIG. 6. (Color online) Intermolecular contribution to the radial distribution function at various shear rates $[(1\times10^{9.0})-(1\times10^{12.0})\ \text{s}^{-1}]$, as obtained from *NPT*-NEMD simulations for *n*-hexadecane at 400 K and 250 MPa. Horizontal line: The density is uniform, $g(r)=1$.

1. Shear rate-induced variation

Following to Eq. (1), we easily computed the RDF for intermolecules, $g(r)$. Figure 6 presents the $g(r)$ curves that were obtained over a wide range of shear rates $(1\times10^{9.0}-1\times10^{12.0}\ \text{s}^{-1})$ from constant-pressure NEMD simulations at 400 K and 250 MPa. First, at short distances $(r<3.08\ \text{Å})$, the value of $g(r)$ was zero because of strong repulsive forces. Next, the first and largest peak occurred at $r\approx5.21$ Å. This local maximum indicated that the probability of finding a pair of molecules with such a separation was highest when the pair potential energy was at a *minimum*.[56,58] The $g(r)$ curve then fell and passed through a minimum value at approximately $r\approx7.43$. The chances of finding a pair of molecules was lower, and its potential energy reached a *maximum* value.[56,58] Finally, at large separations, the potential energy approached *zero* with some fluctuation, so that the density was uniform, i.e., $g(r)\approx1$.[55] This situation revealed that one molecule had no influence on the position of another—namely, there was no long-range order.[56,58]

As a whole, the shapes of the $g(r)$ curves described above for different shear rates clearly represented liquid state characteristics, in accordance with McQuarrie's treatise of statistical mechanics.[56] Significantly, our $g(r)$ curves were in good agreement with the results of Tsuchiya *et al.*,[59] who predicted the melting points of *n*-alkanes using molecular dynamics simulations. In passing, we note that Matteoli and Mansoori[57] proposed a simple expression for the RDFs of pure fluids and mixtures.

In Fig. 6, it is evident that the $g(r)$ curves were affected by the shear rates. At $\dot{\gamma}<1\times10^{11.0}\ \text{s}^{-1}$, there was no correlation between the $g(r)$ curves and the shear rates; in con-

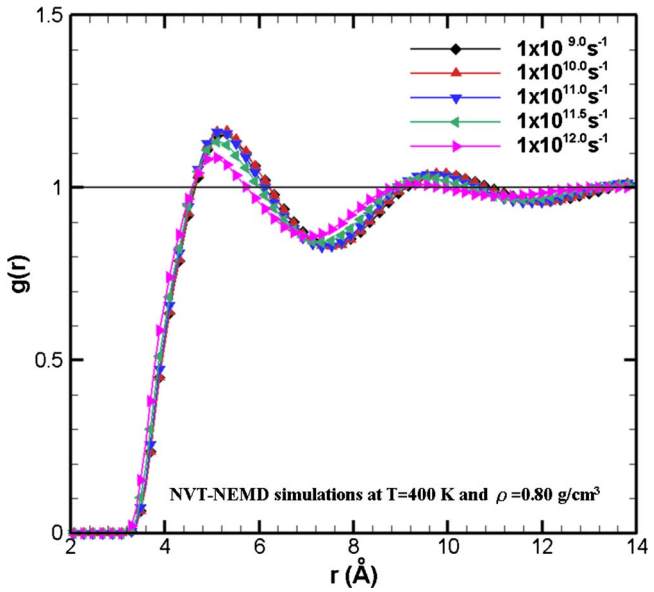

FIG. 7. (Color online) Intermolecular contribution to the radial distribution function at various shear rates $[(1\times10^{9.0})-(1\times10^{12.0})\ \mathrm{s}^{-1}]$, as obtained from *NVT*-NEMD simulations for *n*-hexadecane at 400 K and 0.80 $\mathrm{g/cm}^3$. Horizontal line: The density is uniform, $g(r)=1$.

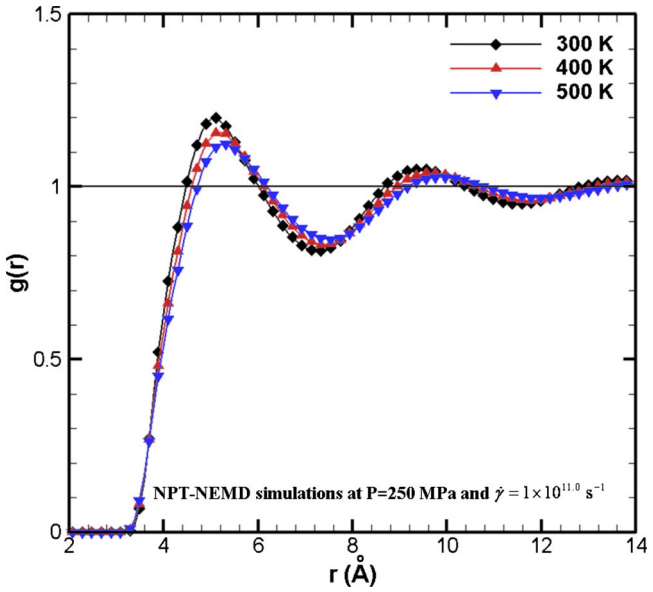

FIG. 8. (Color online) Intermolecular contribution to the RDF at temperatures of 300, 400, and 500 K, as obtained from *NPT*-NEMD simulations for *n*-hexadecane at 250 MPa and $1\times10^{11.0}\ \mathrm{s}^{-1}$. Horizontal line: The density is uniform, $g(r)=1$.

trast, the *intensity* of the first peak at $\dot{\gamma}>1\times10^{11.0}\ \mathrm{s}^{-1}$ decreased upon increasing the shear rate. We noticed that this variation was the same as that observed in the NEMD simulations described by Bosko *et al.* for a dendrimer.[30] Moreover, for a shearing atomic fluid interacting via accurate two-body potentials, Marcelli *et al.*[65] demonstrated that the intensity of the first peak in the $g(r)$ curves at an extreme shear rate (1.95 in reduced units) was specifically lower than that obtained at an equilibrium state. Essentially, the study of the shear rate dependence of RDFs $g(r,\dot{\gamma})$ reported by Koo and Hess[32] revealed that contour diagrams of $g(r,\dot{\gamma})$ obtained at lower shear rates displayed ellipsoidal distortion, whereas a twisted distortion occurred at higher shear rates, i.e., the plot of $g(r,\dot{\gamma})$ became nonspherically symmetrical under extreme shear.

On the other hand, at long distances ($r>10.0$ Å), the $g(r)$ curves tended to gradually approach a value of *one*, with fluctuation, upon increasing the shear rate. Notably, as the shear rate increased, the $g(r)$ curves did not move to either the right or the left. The shifts in the $g(r)$ curves that were manifested at various temperatures, pressures, and densities are discussed below.

Our observations described above imply that at low shear rates, the intermolecular distances remain almost unchanged; in contrast, although shear dilatancy occurs at high shear rates, the intermolecular distances are lengthened upon increasing shear rate. As indicated in Fig. 7, and as expected, the $g(r)$ curves obtained at 400 K and 0.80 $\mathrm{g/cm}^3$ for the constant-volume NEMD systems were the same as those obtained for constant-pressure NEMD systems. In short, whether we employed a constant-volume or constant-pressure NEMD system, the effect of shear dilatancy caused an increase in the intermolecular distance.

2. Temperature-, pressure-, and density-induced variations

In our ensuing RDF discussions, we examined the variations in the $g(r)$ curves under various temperatures, pressures, and densities. Figure 8 presents the $g(r)$ curves obtained at temperatures of 300, 400, and 500 K from constant-pressure NEMD simulations performed at 250 MPa and $1\times10^{11.0}\ \mathrm{s}^{-1}$. Upon increasing the temperature, the intensity of the first peak fell and the overall curve moved to the right. This result signified that the intermolecular distance increased upon increasing the temperature, which was in agreement with Verlet's report of the *equilibrium* MD observation of *liquid argon*.[66]

Figure 9 presents the $g(r)$ curves obtained at 400 K and $1\times10^{11.0}\ \mathrm{s}^{-1}$ over a wide pressure range (50–1000 MPa). With increased pressure, the intensity of the first peak rose and the signals in the curve moved to the left. Thus, the intermolecular distance was clearly shortened upon increasing the pressure; note that this behavior was the exact opposite of the temperature effect in Fig. 8.

Figure 10 displays the $g(r)$ curves obtained at densities of 0.70, 0.80, and 0.90 $\mathrm{g/cm}^3$ from constant-volume NEMD simulations performed at 400 K and $1\times10^{11.0}\ \mathrm{s}^{-1}$. This trend with respect to density was the same as the effect of pressure on the $g(r)$ curves (cf. Fig. 9). Thus, as the density increased, the intermolecular distance decreased correspondingly. In summary, as analyzed above, the changes in $g(r)$ curves caused by changes in temperature, pressure, density, and shear rate contributed to our understanding of common molecular physics. Significantly, the characteristics of our $g(r)$ curves allowed us to ascertain with confidence that our research fluid, *n*-hexadecane, existed in the liquid state under each of the tested sets of conditions.

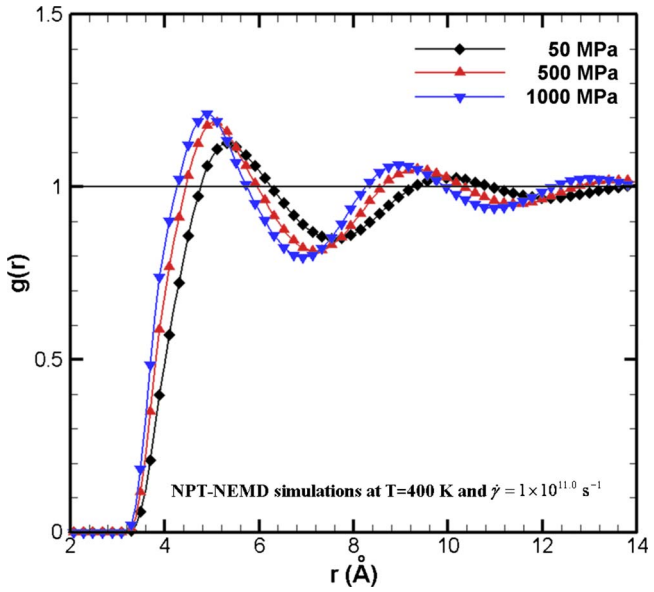

FIG. 9. (Color online) Intermolecular contribution to the radial distribution function at pressures of 50, 500, and 1000 MPa, as obtained from *NPT*-NEMD simulations for *n*-hexadecane at 400 K and $1\times10^{11.0}$ s^{-1}. Horizontal line: The density is uniform, $g(r)=1$.

IV. CONCLUSION

NEMD simulations were used to analyze the shear dilatancy behavior of liquid *n*-hexadecane fluid. Under isothermal conditions, the trends in the rates of shear dilatancy in both constant-volume and constant-pressure NEMD systems agreed well with the *cyclic rule* of pressure P as a function of density ρ and shear rate $\dot{\gamma}$.

To answer the question of why the shear dilatancy of liquid *n*-hexadecane appears in NEMD simulations, we proposed one possible molecular explanation regarding the relationship between the imposed shear rate $\dot{\gamma}$ and the critical shear rate $\dot{\gamma}_c$. For $\dot{\gamma}<\dot{\gamma}_c$, the intermolecular distance did not depend on the shear rate and the fluid's nonequilibrium states were close to equilibrium: i.e., $\rho(\dot{\gamma})\approx\rho(\dot{\gamma}=0)$ under isobaric-isothermal conditions or $P(\dot{\gamma})\approx P(\dot{\gamma}=0)$ under isochoric-isothermal conditions. In contrast, at $\dot{\gamma}>\dot{\gamma}_c$, the intermolecular distance lengthened upon increasing the shear rate; namely, the fluid displayed *shear dilatancy* behavior. In addition, we found that the characteristic shear rate $\dot{\gamma}_m$ is related to the root mean square molecular velocity $\bar{v}_{\mathrm{rms}}$ and the average free molecular distance l_m, namely, $\dot{\gamma}_m=\bar{v}_{\mathrm{rms}}/l_m$.

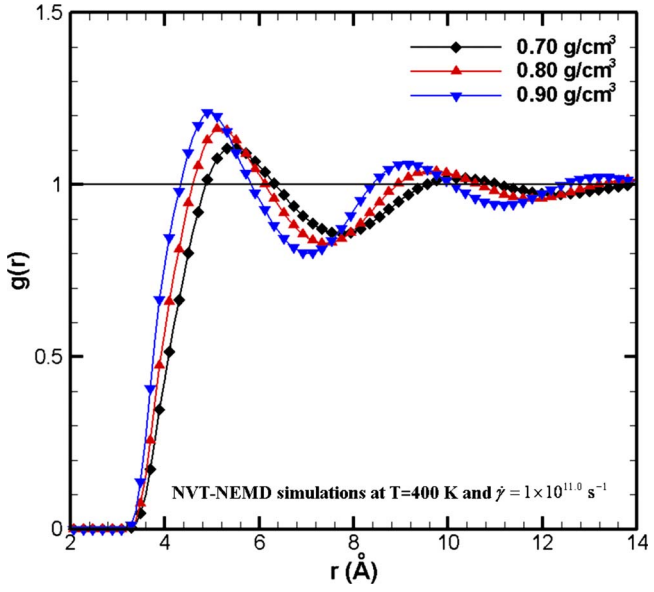

FIG. 10. (Color online) Intermolecular contribution to the RDF at densities of 0.70, 0.80, and 0.90 g/cm^3, as obtained from *NVT*-NEMD simulations for *n*-hexadecane at 400 K and $1\times10^{11.0}$ s^{-1}. Horizontal line: The density is uniform, $g(r)=1$.

Studying the RDFs, we observed variations of the intermolecular distance with respect to the shear rate that were strikingly similar to the variations in the fluid's nonequilibrium states with respect to the shear rate. At low shear rates, the RDF curves bore almost no relation to the shear rate. In contrast, at high shear rates, the *intensity* of the first and highest peaks in the RDF curves *fell* upon increasing the shear rate; this situation provided evidence for an increase in the intermolecular distance. Such variations in intermolecular distances on the molecular level corresponded to nonequilibrium thermodynamic states on the macroscopic scale. Moreover, with rising temperatures, the RDF curves revealed increases in intermolecular distances. On the other hand, upon increasing either pressure or density, we found that the intermolecular distance shortened. Furthermore, the overall characteristics of the RDF curves showed clearly our research fluid existing in the liquid state.

Nonequilibrium thermodynamic state curves, including the $\rho-\dot{\gamma}$ curves presented at different temperatures and pressures and the $P-\dot{\gamma}$ curves presented at different densities, could be normalized to temperature-, pressure-, and density-invariant master curves, respectively. In addition, those master curves could each be formulated using the Cross model. Significantly, the key aspect of the normalization of these master curves was that they could be defined in terms of two relevant characteristic values, i.e., a thermodynamic state variable (a density-characteristic value ρ_C in isobars; a pressure-characteristic value P_C in isochors) and the shear rate. The two criteria for selecting the characteristic values are

(i) Thermodynamic state variable: In both constant-pressure and constant-volume NEMD systems, ρ_C and P_C are given by the equilibrium density ρ_e and the equilibrium pressure P_e, respectively; i.e., $\rho_C=\rho_e$ and $P_C=P_e$.

(ii) Shear rate: In constant-pressure NEMD systems, the shear rate's characteristic value is $\dot{\gamma}_p=a_p\dot{\gamma}_m$, a function of temperature and pressure; $\dot{\gamma}_m$ has a direct connection with the root mean square molecular velocity $\bar{v}_{\mathrm{rms}}$, depending on temperature; $a_p=\sqrt{P/P_0}$ is a shift factor that is related to pressure; P_0 is the reference pressure. Note that at a constant pressure but varying temperatures, all of the shift factors are set to a value of *one* ($a_p=1$). In constant-volume NEMD systems, the shift factor is given by $a_p=\sqrt{P_e(\rho)/P_e(\rho_0)}$, where ρ is the density and its equilibrium pressure is $P_e(\rho)$; ρ_0 is the reference density. More importantly, we obtained that the magnitude of $\dot{\gamma}_c$ in reduced units of

$\dot{\gamma}/\dot{\gamma}_p$ was always close to 0.1, whether dealing with temperature-, pressure-, or density-invariant master curves of nonequilibrium thermodynamic states. Thus, in the particular situation, $\dot{\gamma}/\dot{\gamma}_p \leq 0.1$, the nonequilibrium thermodynamic state approaches equilibrium.

In the near future, we will extend our series of NEMD studies to broaden our understanding with respect to shear dilatancy as it relates to molecular structure: i.e., intramolecular conformations, including bond length, bend angle, and dihedral angle probability distributions, and overall molecular structure, including the radius of gyration, order of orientation, and angle of sphericity.

ACKNOWLEDGMENTS

We are very grateful to the reviewers for their constructive suggestions and thoughtful criticism. We thank the National Science Council of the Republic of China (Grant No. NSC97-2221-E-007-033) and CoreTech System Co., Ltd (Moldex3D) for financial support.

[1] D. J. Evans, Phys. Rev. A **23**, 1988 (1981).
[2] L. M. Hood, D. J. Evans, and H. J. M. Hanley, J. Stat. Phys. **57**, 729 (1989).
[3] K. P. Travis, D. J. Searles, and D. J. Evans, Mol. Phys. **95**, 195 (1998).
[4] J. Ge, G. Marcelli, B. D. Todd, and R. J. Sadus, Phys. Rev. E **64**, 021201 (2001).
[5] A. Berker, S. Chynoweth, U. C. Klomp, and Y. Michopoulos, J. Chem. Soc., Faraday Trans. **88**, 1719 (1992).
[6] J. H. R. Clarke and D. Brown, J. Chem. Phys. **86**, 1542 (1987).
[7] S. T. Cui, S. A. Gupta, P. T. Cummings, and H. D. Cochran, J. Chem. Phys. **105**, 1214 (1996).
[8] P. J. Daivis and D. J. Evans, J. Chem. Phys. **100**, 541 (1994).
[9] P. J. Daivis, D. J. Evans, and G. P. Morriss, J. Chem. Phys. **97**, 616 (1992).
[10] J. Delhommelle and D. J. Evans, J. Chem. Phys. **115**, 43 (2001).
[11] R. Edberg, G. P. Morriss, and D. J. Evans, J. Chem. Phys. **86**, 4555 (1987).
[12] R. Khare, J. de Pablo, and A. Yethiraj, J. Chem. Phys. **107**, 6956 (1997).
[13] J. D. Moore, S. T. Cui, H. D. Cochran, and P. T. Cummings, J. Chem. Phys. **113**, 8833 (2000).
[14] G. P. Morriss, P. J. Daivis, and D. J. Evans, J. Chem. Phys. **94**, 7420 (1991).
[15] C. J. Mundy, J. I. Siepmann, and M. L. Klein, J. Chem. Phys. **103**, 10192 (1995).
[16] H.-C. Tseng, J.-S. Wu, and R.-Y. Chang, J. Chem. Phys. **129**, 014502 (2008).
[17] B. Z. Dlugogorski, M. Grmela, and P. J. Carreau, J. Non-Newtonian Fluid Mech. **48**, 303 (1993).
[18] M. Kröger, W. Loose, and S. Hess, J. Rheol. **37**, 1057 (1993).
[19] Z. Xu, J. J. de Pablo, and S. Kim, J. Chem. Phys. **102**, 5836 (1995).
[20] O. Reynolds, Philos. Mag. **20**, 469 (1885).
[21] M. Reiner and G. W. Scott Blair, in *Rheology: Theory and Applications*, edited by F. R. Eirich (Kluwer Academic, New York, 1967), Chap. 9, p. 461.
[22] D. J. Evans, Int. J. Thermophys. **7**, 573 (1986).
[23] P. A. Thompson and G. S. Grest, Phys. Rev. Lett. **67**, 1751 (1991).
[24] C. Baig, B. J. Edwards, D. J. Keffer, H. D. Cochran, and V. A. Harmandaris, J. Phys. Chem. **124**, 084902 (2006).
[25] P. J. Daivis, M. L. Matin, and B. D. Todd, J. Non-Newtonian Fluid Mech. **147**, 35 (2007).
[26] J. M. Kim, D. J. Keffer, M. Kröger, and B. J. Edwards, J. Non-Newtonian Fluid Mech. **152**, 168 (2008).
[27] K. Kawasaki and J. D. Gunton, Phys. Rev. A **8**, 2048 (1973).
[28] R. B. Bird, R. C. Armstrong, and O. Hassager, *Fluid Mechanics, Dynamics of Polymeric Liquids*, 2nd ed. (Wiley-Interscience, New York, 1987), Vol. 1.
[29] A. Jabbarzadeh, J. D. Atkinson, and R. I. Tanner, Macromolecules **36**, 5020 (2003).
[30] J. T. Bosko, B. D. Todd, and R. J. Sadus, J. Chem. Phys. **121**, 12050 (2004).
[31] J. T. Bosko, B. D. Todd, and R. J. Sadus, J. Chem. Phys. **123**, 034905 (2005).
[32] H.-M. Koo and S. Hess, Physica A **145**, 361 (1987).
[33] N. A. Clark and B. J. Ackerson, Phys. Rev. Lett. **44**, 1005 (1980).
[34] D. J. Evans, H. J. M. Hanley, and S. Hess, Phys. Today **37** (1), 26 (1984).
[35] J.-C. Wang and K. A. Fichthorn, J. Chem. Phys. **109**, 10138 (1998).
[36] H.-C. Tseng, J.-S. Wu, and R.-Y. Chang, J. Chem. Phys. **130**, 084904 (2009).
[37] R. J. Silbey, R. A. Alberty, and M. G. Bawendi, *Physical Chemistry*, 4th ed. (Wiley-Interscience, Hoboken, 2005).
[38] S. Chynoweth and Y. Michopoulos, Mol. Phys. **81**, 133 (1994).
[39] S. Chynoweth, R. C. Coy, and Y. Michopoulos, Proc. Inst. Mech. Eng., Part J: J. Eng. Tribol. **209**, 243 (1995).
[40] M. G. Martin and J. I. Siepmann, J. Phys. Chem. B **102**, 2569 (1998).
[41] J. López-Lemus, M. Romero-Bastida, T. A. Darden, and J. Alejandre, Mol. Phys. **104**, 2413 (2006).
[42] J. P. Nicolas and B. Smit, Mol. Phys. **100**, 2471 (2002).
[43] A. Jabbarzadeh, J. D. Atkinson, and R. I. Tanner, J. Non-Newtonian Fluid Mech. **77**, 53 (1998).
[44] A. Jabbarzadeh, J. D. Atkinson, and R. I. Tanner, J. Chem. Phys. **110**, 2612 (1999).
[45] A. Jabbarzadeh, J. D. Atkinson, and R. I. Tanner, Tribol. Int. **35**, 35 (2002).
[46] H.-C. Tseng, J.-S. Wu, and R.-Y. Chang, "Linear viscoelasticity and thermorheological simplicity of *n*-hexadecane under sinusoidal oscillatory shear via non-equilibrium molecular dynamics simulations," J. Chem. Phys. (submitted).
[47] H.-C. Tseng, J.-S. Wu, and R.-Y. Chang, "Nano-contraction flows of short-chain polyethylene via molecular dynamics simulations," Mol. Simul. (in press).
[48] D. J. Evans and G. P. Morriss, Comput. Phys. Rep. **1**, 297 (1984).
[49] M. P. Allen and D. J. Tildesley, *Computer Simulation of Liquid* (Clarendon, Oxford, 1989).
[50] D. J. Evans and G. P. Morriss, *Statistical Mechanics of Nonequilibrium Liquids* (Cambridge University Press, Cambridge, England, 2008).
[51] A. W. Lees and S. F. Edwards, J. Phys. C **5**, 1921 (1972).
[52] K. P. Travis, P. J. Daivis, and D. J. Evans, J. Chem. Phys. **103**, 10638 (1995).
[53] P. J. Daivis, J. Non-Newtonian Fluid Mech. **152**, 120 (2008).
[54] D. Macgowan and D. M. Heyes, Mol. Simul. **1**, 277 (1988).
[55] J. M. Haile, *Molecular Dynamics Simulation*, 2nd ed. (Wiley-Interscience, New York, 1997).
[56] D. A. McQuarrie, *Statistical Mechanics* (University Science Books, Sausalito, CA, 2000).
[57] E. Matteoli and G. A. Mansoori, J. Chem. Phys. **103**, 4672 (1995).
[58] T. M. Reed and K. E. Gubbins, *Applied Statistical Mechanics: Thermodynamic and Transport Properties of Fluids* (McGraw-Hill, Boston, 1973).
[59] Y. Tsuchiya, H. Hasegawa, and T. Iwatsubo, J. Chem. Phys. **114**, 2484 (2001).
[60] P. J. Daivis, M. L. Matin, and B. D. Todd, J. Non-Newtonian Fluid Mech. **111**, 1 (2003).
[61] M. T. Shaw and W. J. MacKnight, *Introduction to Polymer Viscoelasticity*, 3rd ed. (Wiley-Interscience, Hoboken, 2005).
[62] S. Bair, C. McCabe, and P. T. Cummings, Phys. Rev. Lett. **88**, 058302 (2002).
[63] C. McCabe, C. W. Manke, and P. T. Cummings, J. Chem. Phys. **116**, 3339 (2002).
[64] P. J. Daivis and M. L. Matin, J. Chem. Phys. **118**, 11111 (2003).
[65] G. Marcelli, B. D. Todd, and R. J. Sadus, Phys. Rev. E **63**, 021204 (2001).
[66] L. Verlet, Phys. Rev. **165**, 201 (1968).